Electronic Supplementary Material (ESI) for ChemComm.

Synthesis and Characterization of a Very Low-Coordinate Diferrous $[2Fe\text{-}2S]^0$ Unit

C. Schneider,[a] S. J. Groß, [b] S. Demeshko,[b] S. Bontemps,[c] F. Meyer,[b] C. G. Werncke[a,]*

[a] Philipps-Universität, Fachbereich Chemie, Hans-Meerwein-Straße 4, D-35032 Marburg, Germany

[b] Institute of Inorganic Chemistry, University of Göttingen, Tammannstraße 4, 37077 Göttingen

[c] CNRS, LCC (Laboratoire de Chimie de Coordination), 205 route de Narbonne, 31077 Toulouse and Université de Toulouse, UPS, INPT, 31077 Toulouse, France.

Table of Contents

General considerations

All manipulations were carried out in a glovebox, or using Schlenk-type techniques under a dry argon atmosphere. Used solvents were dried by continuous distillation over sodium metal for several days, degassed via three freeze-pump cycles and stored over molecular sieves 4 Å. The ^{1}H NMR spectra were recorded on a *Bruker AV 500* NMR spectrometers. Chemical shifts are reported in ppm relative to the residual proton signals of the solvent (for ^{1}H) or relative to the signal of the solvent itself (^{13}C). IR measurements were conducted on a *Bruker Alpha ATR-IR* spectrometer. Elemental analysis was performed by the "in-house" service of the Chemistry Department of the Philipps University Marburg, Germany using a CHN(S) analyzer vario MICRO Cube (*Elementar)*.

Solution magnetic susceptibilities were determined by the Evans method[1] Anhydrous $FeCl_2$, $HN(SiMe_3)(Dipp)$, n-butyl lithium (2.5 M in hexane), 18-crown-6, tetramethylsilane (TMS), S_8 and CS_2 were obtained commercially (Sigma-Aldrich, Acros, Strem, Alfa Aesar) and - if not noted otherwise - used as received. CS_2 was degassed, transferred into the glovebox and stored over molecular sieves. 18-crown-6 (18c6) was sublimed prior use to remove traces of water. $K\{18c6\}[Fe(hmds)_2]$[2] (hmds= $N(SiMe_3)_2$)was prepared according to the literature procedure.

1. Synthesis of K{18-crown-6}$_2$[Fe(N(SiMe$_3$)$_2$) (μ_2-S)]$_2$, 1

K{18-crown-6}$_2$[Fe(N(SiMe$_3$)$_2$)$_2$(μ_2-S)]$_2$ (73 mg, 0.05 mmol, 1 equiv.) was dissolved in 2 ml of THF and cooled to -40 °C. Upon the addition of [K{18-crown-6}][Fe(hmds)$_2$] (62 mg, 0.09 mmol, 1.8 equiv.) in THF a slight colour shift from dark red to orange was observable. The mixture was stirred for 1 hour filtered and the filtrate was layered by 2 mL of pentane. Storing the solution at –35 °C for several days led to the precipitation of a dark orange crystalline solid, suitable for X-ray diffraction analysis. Decanting off the supernatant, washing the residue with 2x5 ml of pentane and drying under reduced pressure afforded K{18-crown-6}$_2$[Fe(N(SiMe$_3$)$_2$)(μ_2-S)]$_2$, as a orange crystalline solid (22 mg, 0.020 mmol, 40%).

UV/VIS (THF): λ / nm (ε / L/mol cm) = 505 (1699).

FT-IR (ATR): ($\tilde{\nu}$ / cm^{-1}): $\tilde{\nu}$ = 2941 (w), 2885 (w),2826 (w), 1472 (w), 1453 (w), 1352 (m), 1284 (w), 1232 (m), 1104 (vs), 956 (vs), 867 (s), 825 (vs), 778 (s), 756 (s),747 (m), 711 (m), 658 (s), 610 (m), 552 (m), 529 (w).

CHNS: calc. ($C_{36}H_{84}Fe_2K2N_2O_{12}S_2Si_4$ 1103.42 g/mol): C 39.19 H 7.67 N 2.54 S 5.81 found: C 39.35 H 7.208 N 2.94 S 6.20

^{1}H-NMR: (500.13 MHz, THF-d$_8$, 300 K): δ = 3.50 (C*H*$_2$ 18-crown-6), -2.41 ($w_{1/2}$ = 530.0 Hz, Si*Me*$_3$), ppm.

2. Synthesis of K{18-crown-6}$_2$[Fe(N(SiMe$_3$)$_2$)$_2$(μ_2-S)]$_2$, 2

K(18-crown-6][Fe(N(SiMe$_3$)$_2$)$_2$] (680 mg, 1.0 mmol, 1 equiv.) and Sulfur (32 mg, 1.0 mmol, 1 equiv.) were dissolved in 5 ml of Et2O,leading to an immediate color change of the solution from dark orange to dark red. After stirring for 12 hours the mixture was filtered and the filtrate was stored at -20 °C for several days, which led to the precipitation of a dark red crystalline solid, suitable for x-ray diffraction. The crystals were isolated by filtration, washed twice with 5 ml of pentane and dried under reduced pressure. K{18-crown-6}$_2$[Fe(N(SiMe$_3$)$_2$)$_2$(μ_2-S)]$_2$ could be afforded as a dark red crystalline solid (425 mg, 0.3 mmol, 60%).

FT-IR (ATR): ($\tilde{\nu}$ / cm^{-1}): $\tilde{\nu}$ = 2941 (w), 2884 (w), 2620 (w), 1472 (w), 1453 (w), 1352 (m), 1285 (w), 1232 (m), 1105 (vs), 950 (vs), 863 (s), 828 (vs), 777 (s), 754 (m), 712 (m), 654 (s), 611 (m), 529 (w).

CHNS: calc. ($C_{48}H_{120}Fe_2K_2N_4O_{12}S_2Si_8$ 1424.19 g/mol): C 40.48 H 8,49 N 3.93 S 4.50 found: C 40.51 H 7.84 N 3.78 S 3.95

^{1}H-NMR: (300.13 MHz, THF-d$_8$, 300 K): 3.58 (C*H*$_2$ 18-crown-6). No signal for the complex anion of **2** was detected in the region of ± 200 pm, which is attributed to the paramagnetic nature of Fe^{3+}.

3. Synthesis of K{18-crown-6}[(N(SiMe$_3$)$_2$)$_2$Fe^{III}CS$_3$], 3

K{18-crown-6}$_2$[Fe(N(SiMe$_3$)$_2$)$_2$(μ_2-S)]$_2$ (50 mg, 0.035 mmol, 1 equiv.) was dissolved in 2 mL of THF. The slow addition of CS_2 (21 µl, 0.35 mmol, 10 equiv.) led to a colour change of the solution from red to clear red. After stirring for 2 hours, the mixture was filtered and the filtrate layered by 2 mL of pentane. Storing the solution at -30 °C yielded to the precipitation of red crystals, suitable for X-ray diffraction Decanting off the supernatant, washing of the residue with 2x2 mL of pentane and drying in vacuo afforded **3** as a red crystalline solid (22 mg, 0.028 mmol, 40%).

^{1}H-NMR: (500.13 MHz, THF-d$_8$, 300 K): δ = 17.58 (Si*Me*$_3$), 3.68 (C*H*$_2$ 18-crown-6) ppm.

FT-IR (ATR): ($\tilde{\nu}$ / cm^{-1}): $\tilde{\nu}$ = 1947 (w), 2892 (m), 1472 (w), 1350 (m), 1283 (w), 1240 (s), 1103 (vs), 998 (s), 961 (m), 918 (s), 876 (vs), 832 (s), 783 (m), 757 (m), 705 (m), 667 (s), 613 (w).

UV/VIS (THF): λ / nm (ε / L/mol cm) = 610 (205).

CHNS: calc. ($C_{25}H_{60}KFeN_2Si_4S_3$ 1137.61 g/mol): C 38.1 H 7.67 N 3.55 S 12.2
found: C 37.93 H 7.454 N 3.89 S 11.6.

4. UV/VIS Spectra

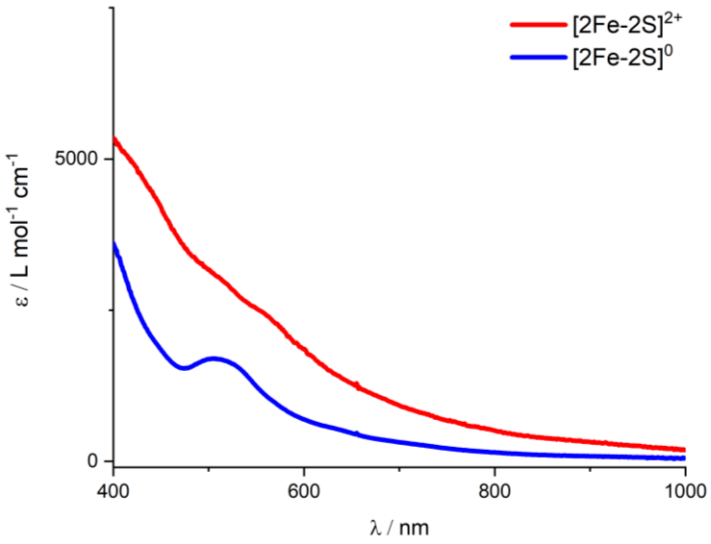

Figure S1. Overlay of the UV/VIS spectra of **2** (red), **1** (blue) in THF at room temperature.

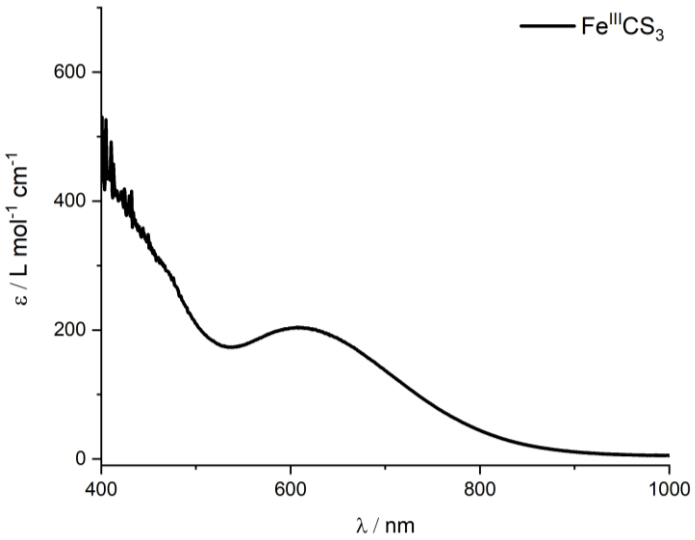

Figure S2. UV/VIS spectrum of [K(18-crown-6)][$(hmds)_2Fe^{III}(CS_3)$] **3** in THF.

5. Cyclic voltammetry

The redox behavior of **2** was examined by cyclic voltammetry. A microcell HC "closed" stand (rhd instruments) was used in combination with a temperature controller (rhd instruments) and an AUTOLAB PGSTAT 204 (Metrohm GmbH) potentiostat/galvanostat. The measurements were performed at 25±0.1 °C, using a TSC 1600 Closed (rhd instruments) glassy carbon cell in a three-electrode configuration with an Ag wire acting as pseudo reference electrode and a glassy carbon working electrode. To secure reproducible conditions the electrodes were freshly polished, rinsed with THF and dried *in vacuo* for 2 hours. 2 mM of analyte and 0.1 M $^nBu_4N[PF_6]$, which acted as electrolyte, were used in the default measurement setup. The $[FeCp_2]$ / $[FeCp_2]^+$ (Fc/Fc^+) redox couple was utilized as internal standard. The measurements were performed at four different scan rates (50, 100, 200, 300, 400 and 500 mV/s), with two full cycles per scan rate. However, due to the fast decomposition of **2** under the measurement conditions it was not possible to get reliable voltammograms at scan rates < 200 mV/s. Peak potentials and currents of of each measurement were determined using the NOVA Software (ver. 1.10.1.9, Metrohm GmbH).

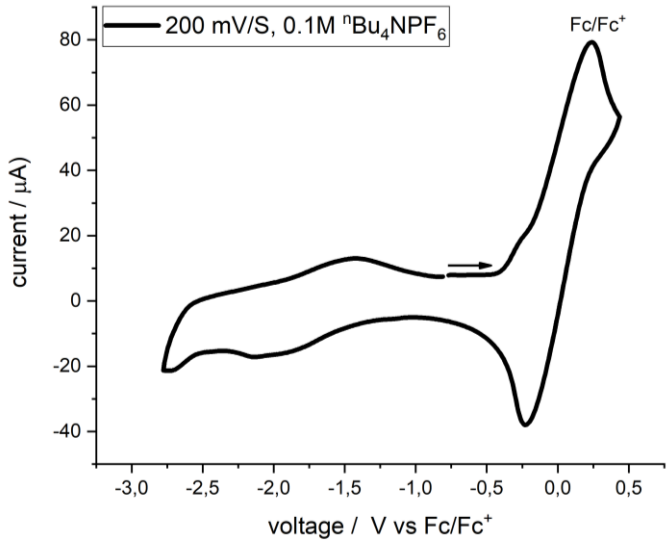

Figure S3. Cyclic voltammogram of $[2Fe\text{-}2S]^{2+}$ **2** in THF at a scan rate of 200 mV/s (0.1 M NBu_4PF_6, vs. Fc/Fc^+) in the presence of ferrocene.

The cyclic voltammogram shows a reduction at -2.12 V and an oxidation at -1.53 V (versus Fc/Fc^+). Due to a peak potential difference of 60 mV and a ratio of the anodic and cathodic peak current $\frac{i_{pa}}{i_{pc}}$= 1.4 the redox event can be described as a quasireversible redox process, which is coupled to a subsequent chemical reaction. The irreversible oxidation at -0.7 V (versus Fc/Fc^+) only showing up in voltammograms with a negative step potential (Figure S4), or in the second cycle (Figure S5) confirms this hypothesis.

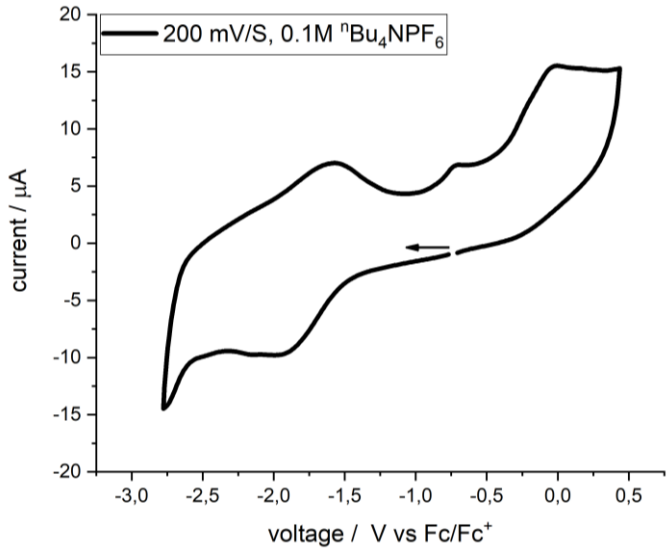

Figure S4. Cyclic voltammogram of $[2Fe\text{-}2S]^{2+}$ **2** in THF at a scan rate of 200 mV/s (0.1 M NBu_4PF_6, vs. Fc/Fc^+) with a negative step potential.

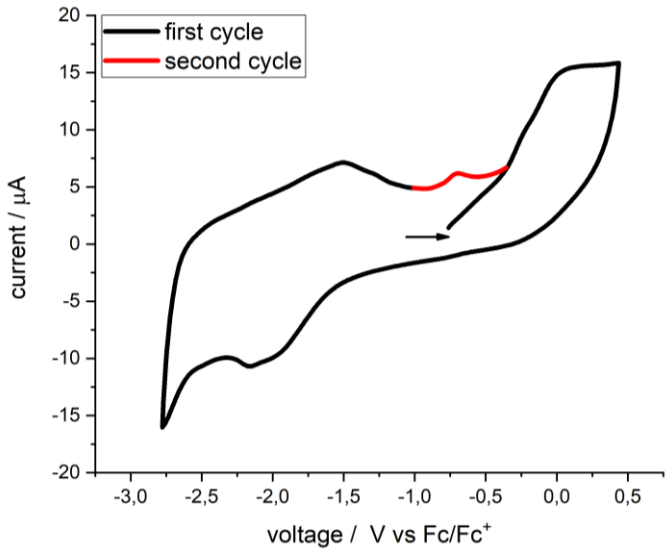

Figure S5. Cyclic voltammogram of $[2Fe\text{-}2S]^{2+}$ **2** in THF at a scan rate of 200 mV/s (0.1 M NBu_4PF_6, vs. Fc/Fc^+) with a positive step potential. The red line represents the start of the second cycle.

6. ^{1}H NMR Spectra

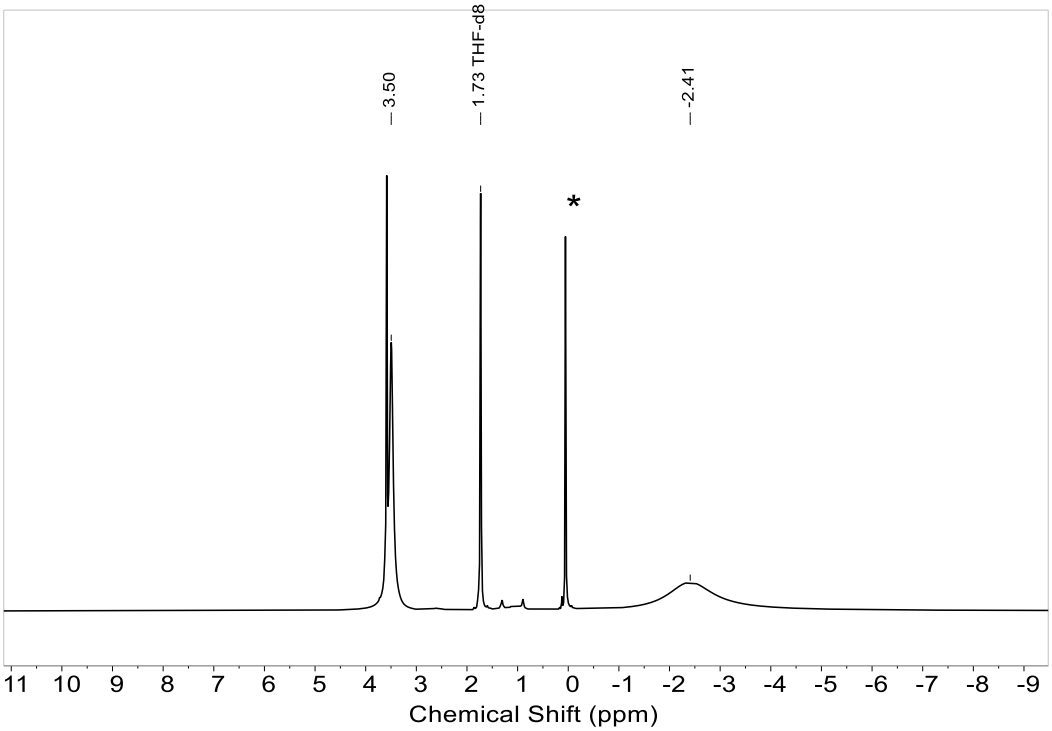

Figure S6. ^{1}H-NMR-spectrum of $[2Fe\text{-}2S]^{0}$ **1** in THF-d_8 (* denotes minor impurities of $HN(SiMe_3)_2$).

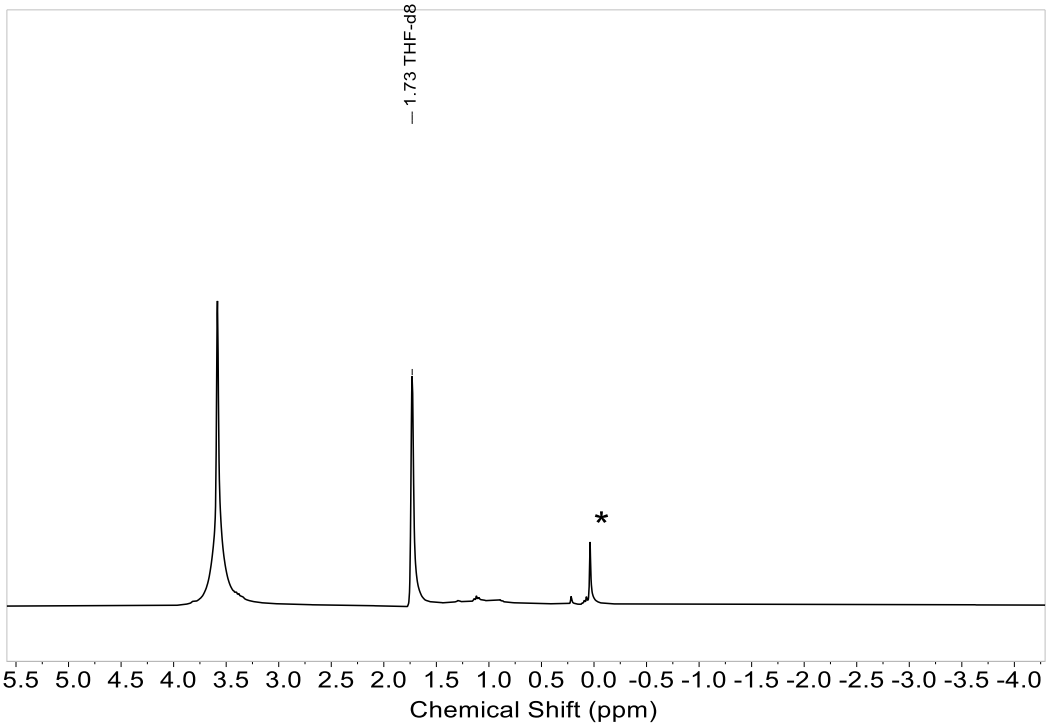

Figure S7. ^{1}H-NMR-spectrum of $[2Fe\text{-}2S]^{2+}$ **2** in THF-d_8 (* denotes minor impurities of $HN(SiMe_3)_2$). Due to the paramagnetic nature of iron(III) no resonances of **2** are detectable. The resonance of the CH_2-groups of the crown ether are overlapped by the THF signal.

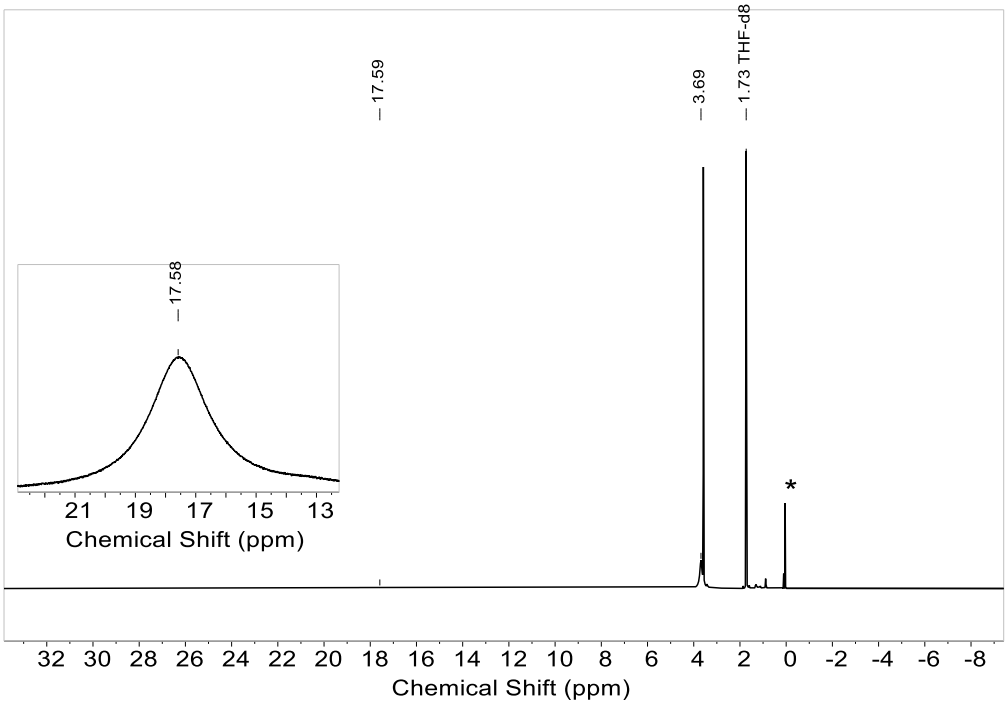

Figure S8. ^{1}H-NMR-spectrum of [K(18-crown-6)][(hmds)$_2$Fe^{III}(CS$_3$)] **3** in THF-d$_8$ (* denotes minor impurities of HN(SiMe$_3$)$_2$).

7. Mössbauer spectroscopy

Mössbauer spectra were recorded with a ^{57}Co source in a Rh matrix using an alternating constant acceleration *Wissel* Mössbauer spectrometer operated in the transmission mode and equipped with a *Janis* closed-cycle helium cryostat. Isomer shifts are given relative to iron metal at ambient temperature. Simulation of the experimental data was performed with the *Mfit* program using *Lorentzian* line doublets: E. Bill, Max-Planck Institute for Chemical Energy Conversion, Mülheim/Ruhr, Germany.

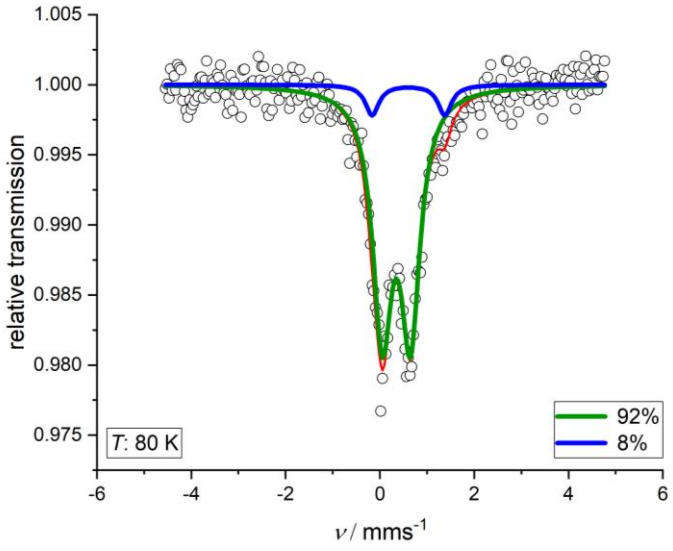

Figure S9. Zero field ^{57}Fe Mössbauer spectrum of solid **2** at 80 K. The green line represents a fit with δ = 0.35 mm/s, $|\Delta E_Q|$ = 0.60 mm/s, which can be assigned to **2**. The blue line represents a fit with δ =

0.61 mm/s, $|\Delta E_Q|$ = 1.51 mm/s, which can be assigned to an unknown impurity or decomposition product.

8. Magnetic Susceptibility Measurements

Temperature-dependent magnetic susceptibility measurements were carried out with a *Quantum-Design* MPMS3 SQUID magnetometer equipped with a 7 Tesla magnet in the range from 295 to 2.0 K at a magnetic field of 0.5 T. The powdered samples were contained in a polycarbonate capsule and fixed in a non-magnetic sample holder. For **1**, the raw data file for the measured magnetic moment was corrected for the diamagnetic contributions of the polycarbonate capsule by subtraction of the raw response functions using the mpView.1.4.1 program: E. Bill, Max-Planck Institute for Chemical Energy Conversion, Mülheim/Ruhr, Germany. For **2**, the raw data file for the measured magnetic moment was corrected for the diamagnetic contribution of the polycarbonate capsule with experimentally obtained gram susceptibilitiy of the polycarbonate capsule. The molar susceptibility data were corrected for the diamagnetic contribution.

Simulation of the experimental magnetic data was performed with the *julX* program: E. Bill, Max-Planck Institute for Chemical Energy Conversion, Mülheim/Ruhr, Germany.

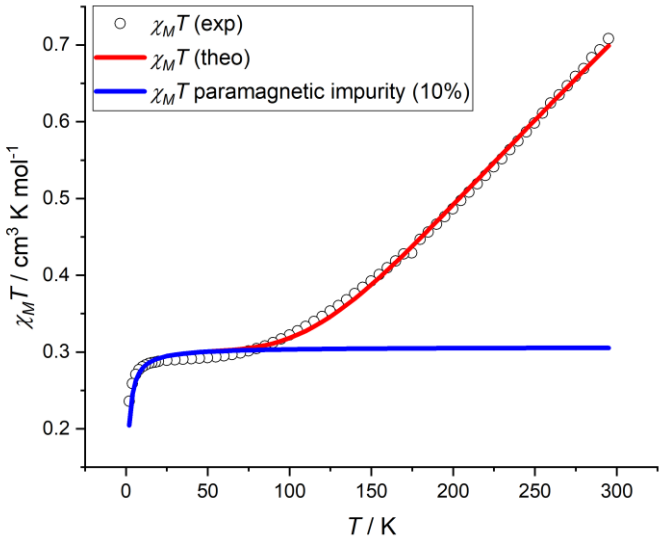

Figure S10. Plot of $\chi_M T$ vs. temperature for diferric cluster **2** at an applied field B = 0.5 T. The red line represents the best fit with the parameters $S_1 = S_2 = 5/2$, $J = = -187$ cm^{-1}, $g_1 = g_2 = 2.15$. The blue line represents a paramagnetic impurity PI (monomeric iron(III), $S = 5/2$).

9. X-Ray diffraction analysis and molecular structures

Data for **1** (CCDC 2097906), **2** (CCDC 2097907), **3** (CCDC 2097908) were collected at 100 K on a Bruker Quest D8 diffractometer using graphite-monochromated Mo-Kα radiation and equipped with an *Oxford Instrument Cooler Device*. The structures have been solved using either OLEX SHELXT V2014/1[3] and refined by means of least-squares procedures on a F^2 with the aid of the program SHELXL-2016/6. include in the softwares package WinGX version 1.63[4] or using CRYSTALS.

The Atomic Scattering Factors were taken from *International Tables for X-Ray Crystallography*[5]. All non-hydrogen atoms were refined anisotropically. All hydrogens atoms were refined by using a riding model. Absorption corrections were introduced by using the MULTISCAN program. Drawings of molecules are performed with the program DIAMOND with 50% probability displacement ellipsoids for non-H atoms. Depiction of H atoms is omitted for clarity.

Table S1. Crystal data and structure refinement for $[2Fe\text{-}2S]^0$ **1**.

Empirical formula	$C_{36}H_{80}Fe_2K_2N_2O_{12}S_2Si_4$
Formula weight	1099.40
Temperature/K	100.0
Crystal system	monoclinic
Space group	P21/n
a/Å	14.4769(8)
b/Å	10.6369(6)
c/Å	20.1652(11)
α/°	90
β/°	96.305(2)
γ/°	90
Volume/Å3	3086.4(3)
Z	2
ρcalcg/cm3	1.183
μ/mm-1	0.796
F(000)	1168.0
Crystal size/mm3	0.456 × 0.187 × 0.12
Radiation	MoKα (λ = 0.71073)
2Θ range for data collection/°	4.064 to 54.36
Index ranges	-18 ≤ h ≤ 18, -13 ≤ k ≤ 13, -25 ≤ l ≤ 25
Reflections collected	86212
Independent reflections	6845 [R_{int} = 0.0457, R_{sigma} = 0.0218]
Data/restraints/parameters	6845/0/277
Goodness-of-fit on F2	1.040
Final R indexes [I>=2σ (I)]	R1 = 0.0327, wR2 = 0.0828
Final R indexes [all data]	R1 = 0.0421, wR2 = 0.0871
Largest diff. peak/hole / e Å-3	0.78/-0.77

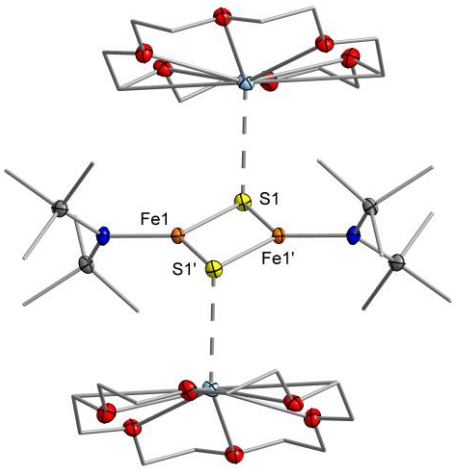

Figure S11. Molecular structure of **1** within the crystal. Hydrogen atoms have been omitted for clarity.

Table S2. Crystal data and structure refinement for $[2Fe\text{-}2S]^{2+}$ **2**.

Empirical formula	$C_{50}H_{125}Fe_2K_2N_4O_{12.5}S_2Si_8$
Formula weight	1461.27
Temperature/K	100.0
Crystal system	triclinic
Space group	P-1
a/Å	12.2287(5)
b/Å	13.8939(6)
c/Å	24.4874(10)
α/°	96.877(2)
β/°	100.9140(10)
γ/°	102.872(2)
Volume/Å3	3925.2(3)
Z	2
ρcalcg/cm3	1.236
μ/mm-1	0.701
F(000)	1574.0
Crystal size/mm^3	0.561 × 0.372 × 0.359
Radiation	MoKα (λ = 0.71073)
2Θ range for data collection/°	4.192 to 58.016
Index ranges	-16 ≤ h ≤ 16, -18 ≤ k ≤ 18, -33 ≤ l ≤ 33
Reflections collected	123101
Independent reflections	20844 [R_{int} = 0.0688, R_{sigma} = 0.0516]
Data/restraints/parameters	20844/2/772
Goodness-of-fit on F2	1.036
Final R indexes [I>=2σ (I)]	R1 = 0.0391, wR2 = 0.0714
Final R indexes [all data]	R1 = 0.0615, wR2 = 0.0769

* The empirical formula differs from $C_{48}H_{125}Fe_2K_2N_4O_{12}S_2Si_8$ due to a non-coordinating Et_2O molecule with chemical occupancy of 50% in the asymmetrical unit.

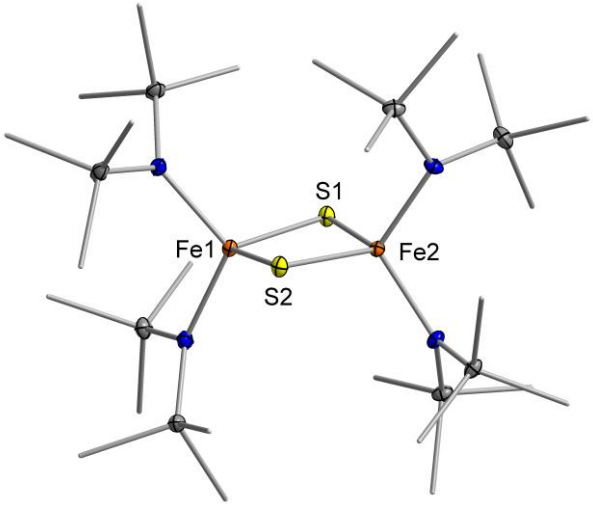

Figure S12. Molecular structure of **2** within the crystal. Hydrogen atoms and the $[K^+(18\text{-crown-6})]$ cations and 0.5 eq. of Et_2O have been omitted for clarity.

Table S3. Crystal data and structure refinement for **3**.

Empirical formula	$C_{25}H_{58}FeKN_2O_6S_3Si_4$
Formula weight	786.22
Temperature/K	100.0
Crystal system	triclinic
Space group	P-1
a/Å	13.1814(7)
b/Å	17.5638(8)
c/Å	19.7643(9)
α/°	65.2010(10)
β/°	87.0280(10)
γ/°	83.5690(10)
Volume/Å3	4127.6(3)
Z	4
ρcalcg/cm3	1.265
μ/mm-1	0.769
F(000)	1676.0
Crystal size/mm3	0.398 × 0.23 × 0.16
Radiation	MoKα (λ = 0.71073)
2Θ range for data collection/°	4.226 to 50
Index ranges	-15 ≤ h ≤ 15, -20 ≤ k ≤ 20, -23 ≤ l ≤ 23
Reflections collected	63125
Independent reflections	14536 [R_{int} = 0.0964, R_{sigma} = 0.0791]
Data/restraints/parameters	14536/86/861
Goodness-of-fit on F2	0.983
Final R indexes [I>=2σ (I)]	R1 = 0.0531, wR2 = 0.1140
Final R indexes [all data]	R1 = 0.0964, wR2 = 0.1255
Largest diff. peak/hole / e Å-3	0.71/-0.52

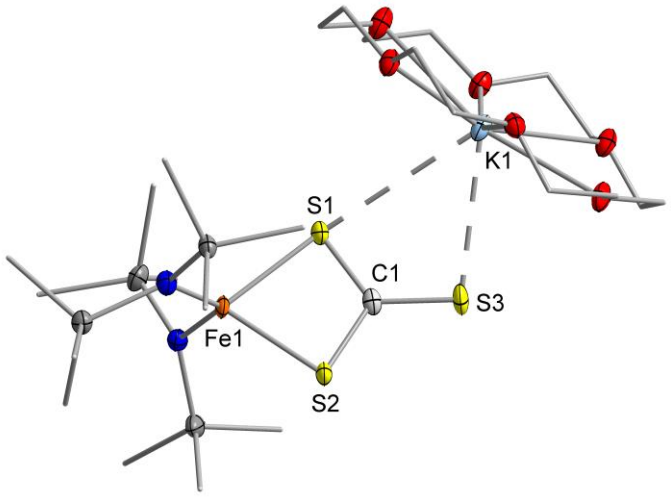

Figure S13. Molecular structure of **3** within the crystal. Hydrogen atoms have been omitted for clarity.

10. References

[1] E. M. Schubert, *Journol Chem. Educ.* **1992**, *69*, 62.

[2] C. Gunnar Werncke, P. C. Bunting, C. Duhayon, J. R. Long, S. Bontemps, S. Sabo-Etienne, *Angew. Chem. Int. Ed.* **2015**, *54*, 245–248.

[3] G. M. Sheldrick, *Acta Crystallogr. Sect. A Found. Crystallogr.* **2015**, *71*, 3–8.

[4] L. J. Farrugia, *J. Appl. Cryst.* **1999**, *32*, 837–838.

[5] Hamilton W. C., *International Tables for X-Ray Crystallography*, Kynoch Press, Birmingham, **1974**.